On the sensitivity of Zero-tail DFT-spread-OFDM to small bandwidth allocations

Berardinelli, Gilberto

Published in:
I E E E Wireless Communications Letters

DOI (link to publication from Publisher):
10.1109/LWC.2017.2784825

Publication date:
2018

Document Version
Accepted author manuscript, peer reviewed version

This article has been accepted for publication in a future issue of this journal, but has not been fully edited. Content may change prior to final publication. Citation information: DOI 10.1109/LWC.2017.2784825, IEEE Wireless Communications Letters

On the sensitivity of Zero-Tail DFT-spread-OFDM to small bandwidth allocations

Gilberto Berardinelli

Department of Electronic Systems, Aalborg University, Denmark
E-mail: gb@es.aau.dk

***Abstract*—The benefits of Zero-tail discrete Fourier transform -spread- orthogonal frequency division multiplexing (ZT DFT-s-OFDM) in terms of spectral containment and link performance subsume that the internal guard period of the waveform has negligible power. However, the effective power of such guard period depends in practice on the bandwidth allocation and is still significant in case of small bands. In this letter, we characterize the residual energy of the ZT DFT-s-OFDM guard period and evaluate its impact on spectral containment, non-cyclic inter-symbol interference (ISI) and link performance when small transmission bands are used. Spectral containment is shown not to be affected thanks to the oscillating part of the guard period, which ensures the presence of low power samples in the transition between adjacent time symbols. Despite the larger tail power, link performance is shown to be only marginally affected. This is because small bandwidth configurations experience a nearly flat fading, and therefore minimum non-cyclic ISI over the next symbol.**

I. Introduction

The Zero-tail discrete Fourier transform - spread - orthogonal frequency division multiplexing (ZT DFT-s-OFDM) waveform copes with the delay spread of the fading channel with an internal low power guard period rather than with a cyclic prefix (CP) [1]. The low power tail of the signal is meant indeed for absorbing the data energy leakage due to the dispersion of the wireless channel, thus avoiding intersymbol interference (ISI) and enabling the possibility of performing efficient one-tap frequency domain equalization at the receiver. The size of the low-power tail can be tuned according to the estimated delay spread of the channel, thus avoiding the inefficiencies of hard-coded CP as used in current Long Term Evolution (LTE)/LTE-Advanced (LTE-A) technologies [2]. ZT DFT-s-OFDM also features attractive properties in terms of peak-to-average power ratio (PAPR) and spectral containment, the latter being particularly attractive for asynchronous transmissions [3].

The benefits of ZT DFT-s-OFDM hold with the assumption that the tail of the signal has nearly zero-power; however, the residual power of the tail depends on the effective bandwidth allocation. Figure 1 shows realizations of ZT-DFT-s-OFDM signals for different numbers of subcarriers (N). While a large bandwidth leads to a significantly low power tail (around 25 dB lower than the average transmit power), for the other cases such power is far from being negligible. A small bandwidth is typically allocated to cell-edge users such that they can benefit from a higher power spectral density. The high residual power of the tail may affect the spectral containment since it introduces power transition between adjacent symbols. Further, it can also impact negatively the link performance since it generates non-cyclic ISI. In previous studies, e.g. [1], [4], [5], the ZT DFT-s-OFDM performance has been mainly evaluated for significantly large bandwidth, which hides the effects of a non-ideal signal tail.

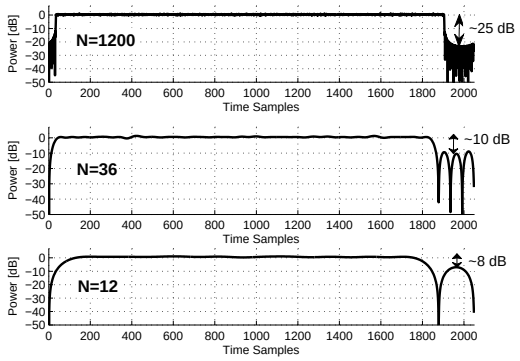

Fig. 1. Low-power tail degradation in ZT DFT-s-OFDM for decreasing bandwidth allocations, assuming N_{FFT}=2048. The residual tail power increases for small bands.

In this letter, we evaluate the sensitivity of ZT DFT-s-OFDM to small bandwidth allocations. We present first an analytical analysis of the residual tail power as a function of the used spectrum resources, and then evaluate spectral containment, residual non-cyclic ISI and link performance for different resource allocations. Our aim is to address whether an internal guard period with non-negligible power has a major negative impact on the ZT DFT-s-OFDM performance.

II. Signal generation

We present here the generation of ZT DFT-s-OFDM signals. Let us define the following $N \times 1$ column vector:

$$\mathbf{q} = \left[\mathbf{0}_{N_{\mathrm{h}}}\, \mathbf{d}^{\mathrm{T}}\, \mathbf{0}_{N_{\mathrm{t}}}\right]^{\mathrm{T}}, \tag{1}$$

where $\mathbf{0}_x$ denotes an x-length vector of zeros, $\mathbf{d}$ is a $(N - N_{\mathrm{h}} - N_{\mathrm{t}}) \times 1$ column vector of data symbols, and $(\cdot)^{\mathrm{T}}$ denotes the transpose operator. The vector $\mathbf{q}$ is fed to a DFT block, whose output is then mapped over a set of frequency subcarriers and IFFT-processed. The resulting $N_{\mathrm{FFT}} \times 1$ time signal column vector $\mathbf{s}$ can be then expressed as:

$$\mathbf{s} = \mathbf{F}_{N_{\mathrm{FFT}}}^{-1} \mathbf{M} \mathbf{F}_N \mathbf{q}, \tag{2}$$

This article has been accepted for publication in a future issue of this journal, but has not been fully edited. Content may change prior to final publication. Citation information: DOI 10.1109/LWC.2017.2784825, IEEE Wireless Communications Letters

where $\mathbf{F}_P$ denotes the $P \times P$ DFT matrix, i.e. $\mathbf{F}_P[a,b] = \frac{1}{\sqrt{P}} e^{-\frac{j2\pi ab}{P}}$, for $a = 0, \cdots, P-1$, $b = 0, \cdots, P-1$ and $\mathbf{M}$ is the $N_{\mathrm{FFT}} \times N$ matrix which maps the data on the frequency subcarriers. The j-th row $\mathbf{m}_j$ of $\mathbf{M}$, with $j = 0, \cdots, N_{\mathrm{FFT}}-1$, is defined as follows:

$$\mathbf{m}_j = \begin{cases} \mathbf{e}_j & \text{if } j \in S \\ \mathbf{0}_N & \text{if } j \notin S \end{cases}$$

where S denotes the set of indexes of the used frequency subcarriers, and $\mathbf{e}_j$ is an N-sized unit vector consisting of all zeros except a 1 in the *j*th position. A localized subcarrier mapping is here considered, i.e. data is allocated over a contiguous set of subcarriers. It is known that a cascade of DFT, subcarrier mapping and IFFT blocks correspond to a Dirichlet filter which localizes the significant part of the energy of each input data symbol in a specific output sample [6]. In particular, most of the energy of the data symbol at position z in the data array falls in the position $\lceil zN_{\mathrm{FFT}}/N \rceil$ of the time domain $\mathbf{s}$ vector, where $\lceil x \rceil$ denotes the nearest integer number higher than x. As a consequence, the pre-DFT vectors $\mathbf{0}_{N_{\mathrm{h}}}$ and $\mathbf{0}_{N_{\mathrm{t}}}$ will be spread over the head and the tail of $\mathbf{s}$. The length of the $\mathbf{s}_{\mathrm{h}}$ and $\mathbf{s}_{\mathrm{t}}$ vectors, representing the corresponding time domain head/tail parts of $\mathbf{s}$, is given by $N_{\mathrm{s_h}} = \lceil N_{\mathrm{h}} N_{\mathrm{FFT}}/N \rceil$ and $N_{\mathrm{s_t}} = \lceil N_{\mathrm{t}} N_{\mathrm{FFT}}/N \rceil$, respectively.

Realizations of the time domain signals for different N values are shown in Figure 1. The vectors $\mathbf{s}_{\mathrm{h}}$ and $\mathbf{s}_{\mathrm{t}}$ are the low power vectors (rather than *zero*-power vectors) since they collect the energy leakage of the data part of the signal due to the response of the Dirichlet filter. The low power tail is meant at coping with the delay spread of the channel within the symbol itself; non-cyclic ISI is therefore reduced to the energy spillover of the tail to the next symbol. The low power head is instead meant at avoiding power regrowth of the data part in the last samples of the symbol due to the cyclicity of IFFT operation [3]; it then represents a pure overhead term. It is worth to observe that the usage of low power head and tail vectors smoothens the abrupt transitions between adjacent time symbols; this is shown to reduce the out-of-band emissions of the signals with respect to baseline CP OFDM/DFT-s-OFDM.

The generated signal vector is then transmitted over the air at a sample rate $S = N_{\mathrm{FFT}} \Delta f$, where Δf denotes the subcarrier spacing. In case of ideal unitary channel response and absence of Gaussian noise, the transmit vector $\mathbf{q}$ can be retrieved as $\mathbf{q} = \mathbf{F}_N^{-1} \mathbf{M}^{-1} \mathbf{F}_{N_{\mathrm{FFT}}} \mathbf{r}$, where $\mathbf{r} = \mathbf{s}$ denotes the received signal. The original data vector is obtained by discarding the head and tail sequences, i.e. $\mathbf{d} = \mathbf{q}[N_{\mathrm{h}} : (N - N_{\mathrm{t}} - 1)]$.

In case of transmission over a fading channel, the receive signal reads $\mathbf{r} = \mathbf{s} \otimes \mathbf{h}$, where $\mathbf{h}$ is the channel impulse response with delay spread τ, and $\otimes$ denotes the linear convolution operator. Due to the delay spread of the channel part of the energy of the tail of the symbol will be leaking to the next symbol. Such non-cyclic ISI affects not only the next symbol of the intended user, but the entire operational bandwidth, and therefore also simultaneously active users in neighboring frequency chunks. The non-cyclic ISI component affecting the entire operational bandwidth is given by $\overline{\mathbf{Z}} = \mathbf{F}_{N_{\mathrm{FFT}}} \mathbf{r}_\tau$, where $\mathbf{r}_\tau = [\mathbf{r}(N_{\mathrm{FFT}} : N_{\mathrm{FFT}} + N_\tau - 1)\ \mathbf{0}_{N_{\mathrm{FFT}} - N_\tau}]$, with $N_\tau = \lceil \tau / S \rceil$. For the rest of the letter, we only focus on the impact of the non-cyclic ISI to the intended user. Multi-user aspects of small bandwidth allocations with ZT DFT-s-OFDM are left for future work. The non-cyclic ISI component of the intended user can be calculated as $\mathbf{Z} = \mathbf{F}_{\mathrm{N}}^{-1} \mathbf{M}^{-1} \mathbf{F}_{N_{\mathrm{FFT}}} \mathbf{r}_\tau$. Its component on the data vector is then given by $\mathbf{z} = \mathbf{Z}[N_{\mathrm{h}} : (N - N_{\mathrm{t}} - 1)]$, and its overall power can be calculated as $P_{\mathrm{ISI}} = \sum_{i=0}^{N-N_{\mathrm{h}}-N_{\mathrm{t}}} |\mathbf{z}(i)|^2$.

III. Tail analysis

In this section, we analyze the residual energy leakage on the tail of the signal. Let $N_{\mathrm{s_0}}$ denote the total length of the internal guard period, i.e. $N_{\mathrm{s_0}} = N_{\mathrm{s_h}} + N_{\mathrm{s_t}}$. Without loss of generality, we assume for the moment that $N_{\mathrm{h}} = N_{\mathrm{s_h}} = 0$ and focus on the generation of $\mathbf{s}_{\mathrm{t}}$. By defining the matrix $\mathbf{V} = \mathbf{F}_{N_{\mathrm{FFT}}}^{-1} \mathbf{M} \mathbf{F}_N$, we can write $\mathbf{s} = \mathbf{V}\mathbf{q}$, and $\mathbf{s}_{\mathrm{t}} = \tilde{\mathbf{V}}\mathbf{d}$, where $\tilde{\mathbf{V}} = \mathbf{V}(N_{\mathrm{FFT}} - N_{\mathrm{s_t}} : N_{\mathrm{FFT}} - 1, 0 : N - N_{\mathrm{t}} - 1)$. The vector of the average power of $\mathbf{s}_{\mathrm{t}}$ is then given by:

$$\mathbf{p}_{\mathrm{s_t}} = \mathrm{E}\left\{\mathrm{diag}\left(\mathbf{s}_{\mathrm{t}} \mathbf{s}_{\mathrm{t}}^{\mathrm{H}}\right)\right\} = \mathrm{E}\left\{\mathrm{diag}\left(\tilde{\mathbf{V}} \mathbf{d}\mathbf{d}^{\mathrm{H}} \tilde{\mathbf{V}}^{\mathrm{H}}\right)\right\}, \quad (3)$$

where $\mathrm{E}\{\cdot\}$ denotes the expectation operation, $(\cdot)^{\mathrm{H}}$ is the Hermitian operator and $\mathrm{diag}(\cdot)$ returns the diagonal of the matrix where it is applied. Since the only random term in (3) is given by the data vector $\mathbf{d}$, it can be rewritten as follows:

$$\mathbf{p}_{\mathrm{s_t}} = \mathrm{diag}\left(\tilde{\mathbf{V}} \mathrm{E}\left\{\mathbf{d}\mathbf{d}^H\right\} \tilde{\mathbf{V}}^H\right). \quad (4)$$

Common data symbol constellations are defined in a way that their average power is unitary, i.e. $\mathrm{E}\left\{\mathbf{d}\mathbf{d}^{\mathrm{H}}\right\} = \mathbf{I}_{N-N_{\mathrm{t}}}$, where $\mathbf{I}_P$ denotes the $P \times P$ identity matrix. The elements of $\mathbf{p}_{\mathrm{s_t}}$ can then be expressed as:

$$\mathbf{p}_{\mathrm{s_t}}(m) = |\mathbf{s}_{\mathrm{t}}(m)|^2 = \sum_{k=0}^{N-N_{\mathrm{t}}-1} \left|\tilde{\mathbf{V}}(m,k)\right|^2, \quad (5)$$

for $m = 0 : N_{\mathrm{s_t}} - 1$. By exploiting the identity $\sin(x) = \left(e^{jx} - e^{-jx}\right)/2j$, it can be shown by straightforward calculations that (5) can be expressed as the product of two functions:

$$\mathbf{p}_{\mathrm{s_t}}(m) = \Theta(m)\,\Phi(m), \quad (6)$$

with

$$\Theta(m) = \sin^2\left(\frac{\pi N (m + N_{\mathrm{FFT}})}{N_{\mathrm{FFT}}}\right), \quad (7)$$

$$\Phi(m) = \frac{1}{N^2} \sum_{k=0}^{N-N_{\mathrm{t}}-1} \csc^2\left(\frac{\pi(m + N_{\mathrm{FFT}} - N_{\mathrm{s_t}})}{N_{\mathrm{FFT}}} - \frac{\pi k}{N}\right). \quad (8)$$

Both Θ and Φ functions are displayed in Figure 2, where the simulation result for $\mathbf{p}_{\mathrm{s_t}}$ is also included for the sake of validation. Θ represents the oscillating part of the tail, while Φ is its envelope. It is clear from (7) that the local minima of Θ are at positions $\left\lceil q \frac{N_{\mathrm{FFT}}}{N} \right\rceil$, for $q = 0, \ldots, N_{\mathrm{t}} - 1$.

The power regrowth at the last samples of Φ is due to the cyclicity of the IFFT which appears in (2). Such power regrowth is known to potentially generate significant ISI

This article has been accepted for publication in a future issue of this journal, but has not been fully edited. Content may change prior to final publication. Citation information: DOI 10.1109/LWC.2017.2784825, IEEE Wireless Communications Letters

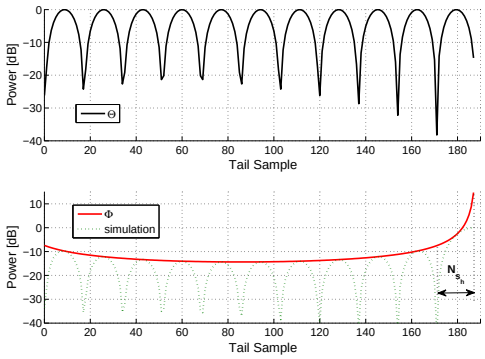

Fig. 2. Oscillating part and envelope of the low power tail, assuming N=120, N_{FFT}=2048 and N_{t}=11 $\rightarrow$ $N_{\mathrm{s_t}}$=188. The green dotted line displays the simulation result for $\mathbf{p}_{\mathrm{s_t}}$.

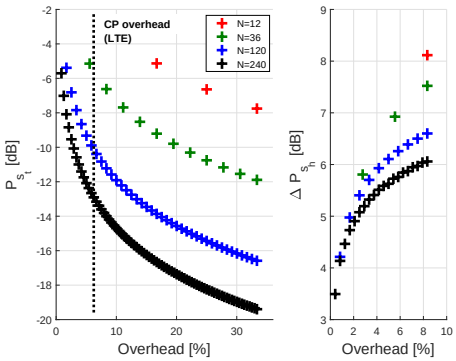

Fig. 3. Overall tail power and power reduction due to head insertion as a function of the tail/head overhead, respectively.

in case of transmission over time dispersive channels. By cyclically shifting the last N_{h} zero samples of the input data vector to its beginning, the last $N_{\mathrm{s_h}}$ samples of Φ are also cyclically shifted to the beginning of the time domain signal, as in Figure 1. The length of the tail and its overall power are therefore diminished, and the power regrowth does not affect the edge of the symbol. As mentioned in Section II, $\mathbf{0}_{N_{\mathrm{h}}}$ is an overhead term and its length should be minimized; however, the head sequence should still be long enough to ensure a low power regrowth. Note that, every pre-DFT zero is mapped over a point in position $\left\lceil q\frac{N_{\mathrm{FFT}}}{N}\right\rceil$ of the time domain signal; in case a N_{h}-length power head is inserted, the transitions between adjacent symbols happen in correspondence of a minimum of the Θ function.

Figure 3 shows the overall power $P_{\mathrm{s_t}}$ of the tail, i.e. $P_{\mathrm{s_t}} = \sum_{q=0}^{N_{\mathrm{s_0}}-1} \mathbf{p}_{\mathrm{s_t}}(m)$ as a function of the $N_{\mathrm{s_0}}$ overhead with respect to the N_{FFT}-length symbol. For the smallest bandwidth allocation (12 subcarriers, corresponding to a Physical Resource Block (PRB) in the LTE numerology [2]) the minimum overhead is 16,67% corresponding to N_{t}=N_{h}=1; this is higher than the CP overhead in LTE ($\sim$6.7% for the short CP configuration), also highlighted in the figure. Larger bandwidth allocations allow for a lower minimum overhead, still leading though to significant tail power (around $\sim$-5 dB). The minimum tail power diminishes by tolerating a larger overhead. As already shown in Figure 1, larger bands lead to a lower minimum power, therefore closely coping with the assumption of nearly-zero tail power. The energy reduction $\Delta P_{\mathrm{s_h}}$ in the tail due to the introduction of a zero-head N_{h}, i.e. $\Delta P_{\mathrm{s_h}} = P_{\mathrm{s_t}} - \sum_{q=N_{\mathrm{s_0}}-N_{\mathrm{s_h}}}^{N_{\mathrm{s_0}}-1} \mathbf{p}_{\mathrm{s_t}}(q)$ as a function of the N_{h} overhead is also shown in Figure 3 for different bandwidth configurations, assuming an $N_{\mathrm{s_t}}$ length equal to the closest value larger than the CP length in LTE. For the 12 subcarriers case, the minimum overhead is 8.33% (corresponding to N_{h}=1); such configuration leads to the highest energy reduction compared to the other configurations for the same overhead. While the overall energy in the tail diminishes in case of larger bandwidth allocations, the insertion of a low power head is more beneficial for small bandwidth allocations.

IV. Simulation Results

We evaluate here spectral containment, residual non-cyclic ISI and link performance of ZT DFT-s-OFDM for different bandwidth allocations with Monte Carlo simulations. In order to have a fair comparison, when not differently specified the overhead of N_{h} and N_{t} is designed to be the same as the minimum for the 12 subcarriers case for all the bandwidth configurations, i.e. N_{h}=N_{t}=8.33%. CP DFT-s-OFDM is also included in the results for the sake of comparison, assuming a CP length N_{CP} equal to $N_{\mathrm{s_t}}$. We assume N_{FFT}=2048, and Δf= 15 kHz, corresponding to the LTE settings for a 20 MHz system bandwidth [2]. For ZT DFT-s-OFDM, a 15 symbols frame configuration is assumed, while for CP DFT-s-OFDM an LTE-like configuration with 14 symbols is used.

The spectral containment performance of ZT DFT-s-OFDM is shown in Figure 4. The same transmit power for all configurations is assumed. The ZT DFT-s-OFDM configurations reach similar out-of-band emissions, significantly lower than CP DFT-s-OFDM. The attractive spectral containment property of ZT DFT-s-OFDM is then not affected by the small bandwidth allocation, despite of the non-negligible tail power. This is due to the fact that the transition between the tail of a symbol and the head of a consecutive one, happens in the position of the local minima of the Θ function in (7), and is therefore only marginally affected by the eventual significant envelope power Φ.

Residual ISI and link performance are studied by considering a frequency selective channel with six taps and exponential power delay profile $h(t) = (1/\tau_{\mathrm{rms}})\, e^{-t/\tau_{\mathrm{rms}}}$, where τ_{rms} denotes the root mean square delay spread. The empirical cumulative distribution function (ECDF) of the residual non-cyclic ISI calculated as described in Section II is shown in Figure 5, considering channels with different τ_{rms}. Note that, for CP DFT-s-OFDM the residual non-cyclic ISI is 0 by construction, and therefore not shown in the figure. For the case of a low dispersive channel ($\tau_{\mathrm{rms}} = 0.34\ \mu s$, leading to a $\sim 1\ \mu s$ excess delay), the residual ISI power is very low but clearly increases with the bandwidth size, especially when moving from $N = 12$ to $N = 36$. Despite of the higher tail power, the $N = 12$ configuration experiences indeed a nearly flat fading which translates to a low energy leakage. The ISI

This article has been accepted for publication in a future issue of this journal, but has not been fully edited. Content may change prior to final publication. Citation information: DOI 10.1109/LWC.2017.2784825, IEEE Wireless Communications Letters

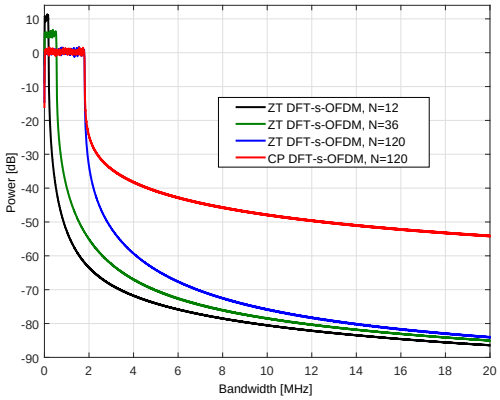

Fig. 4. Spectral containment of ZT DFT-s-OFDM.

energy increases for all the configurations in case of a channel with $\tau_{\text{rms}} = 1\ \mu s$ (leading to a $\sim 3\ \mu s$ excess delay), and the gap is here diminished. The small bandwidth allocation is more sensitive to the time dispersion of the channel as compared to larger allocations, i.e., the interference increases more rapidly as the delay spread increases. Nevertheless, the amount of the interference for the cases with small bandwidth allocations (i.e., even though the tail power is larger) can be still less than the cases with larger allocations since the channel appears to be flat in the first case. For example, the $N = 120$ configuration experiences here slightly lower ISI than $N = 36$. The case of a short head (N_{h} having 4.16% overhead) for $N = 120$ is also included in Figure 5, in order to highlight the sensitivity of the performance with respect to the head size.

The link performance is studied by considering the channel with $\tau_{\text{rms}} = 1\ \mu s$. A 2 GHz carrier frequency is assumed, and a 3 kmph speed. Data bits are encoded and interleaved according to the LTE Release 8 specifications [7]. Full channel knowledge at the receiver is assumed as well as single-tap minimum mean square error (MMSE) equalization. Figure 6 displays the block error rate (BLER) performance. Note that, for CP DFT-s-OFDM, $\text{E}_\text{S}/\text{N}_0$ is corrected of a factor equal to $(N_{\text{FFT}} + N_{\text{CP}})/N_{\text{FFT}}$, to account for the CP losses. In case of quadrature phase shift keying (QPSK) modulation with 1/2 coding rate, performance of ZT DFT-s-OFDM and CP DFT-s-OFDM are approximately the same for the different configurations. However, a significant degradation appears for the 16QAM (16 quadrature amplitude modulation) 4/5 case. This is because the non-ideal tail has a higher power than noise at high $\text{E}_\text{S}/\text{N}_0$ and therefore impacts on the signal cyclicity. The degradation is higher for the $N = 36$ and $N = 120$ configurations, due to the higher residual ISI as highlighted in Figure 5, and further increased in the case of a shorter head (N_{h} with 4.16% overhead). The high coding rate is inefficient for counteracting such residual ISI.

V. Conclusions

In this letter, we have evaluated the sensitivity of ZT DFT-s-OFDM to small bandwidth allocations. We have decomposed

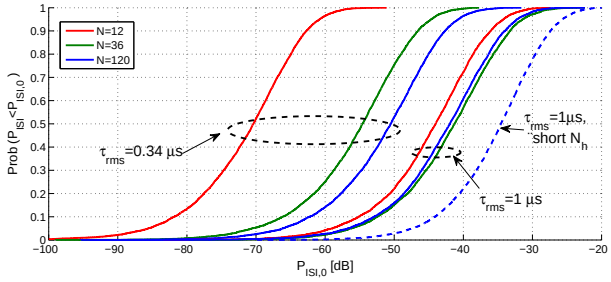

Fig. 5. Non-cyclic residual ISI power for ZT DFT-s-OFDM.

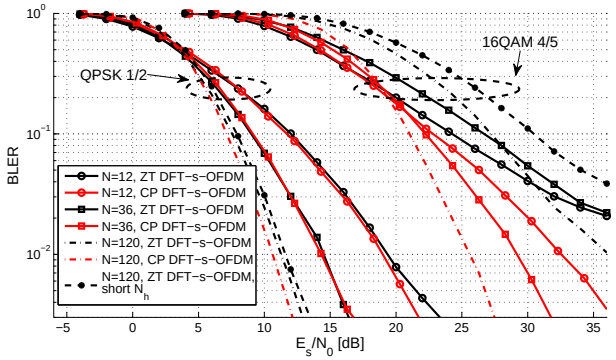

Fig. 6. BLER performance.

the signal tail in its oscillating and envelope parts. Small band allocations are shown not to affect the spectral containment of the waveform, since the transitions between adjacent symbols happen in proximity of the local minima of the oscillating part of the tail, provided a low power head is included. Link performance reflects the trade-off between large tail power and low energy dispersion, leading ultimately to a lower degradation than larger bandwidth allocations at high $\text{E}_\text{S}/\text{N}_0$. Future work will analyze the performance of different bandwidth configurations in multi-user scenarios, considering the mutual impact of non-cyclic ISI in both synchronous and asynchronous cases. The potential of frequency domain shaping in reducing the energy in the tail and its impact on the link performance are also to be investigated.

References

[1] G. Berardinelli, F. Tavares, T. B. Sørensen, P. Mogensen, and K. Pajukoski, "Zero-tail DFT-spread-OFDM signals," *IEEE Globecom Workshops*, December 2013.

[2] H. Holma and A. Toskala, *LTE-Advanced: 3GPP Solutions for IMT-Advanced*. Wiley, 2012.

[3] G. Berardinelli, F. Tavares, T. B. Sørensen, P. Mogensen, and K. Pajukoski, "On the potential of Zero-Tail DFT-spread-OFDM in 5G networks," *IEEE 80th Vehicular Technology Conference, VTC2014-Fall*, September 2014.

[4] U. Kumar, C. Ibars, A. Bhorkar, and H. Jung, "A Waveform for 5G: Guard Interval DFT-s-OFDM," *IEEE Globecom Workshops*, December 2015.

[5] A. Sahin, R. Yang, M. Ghosh, and R. L. Olesen, "An Improved Unique Word DFT-Spread OFDM scheme for 5G Systems," *IEEE Globecom Workshops*, December 2015.

[6] G. H. Myung and J. D. Goodman, *Single Carrier FDMA - A New Air Interface for Long Term Evolution*. John Wiley, 2008.

[7] "Multiplexing and channel coding," 3rd Generation Partnership Project, Tech. Rep. TR 25.212, V8.0.0, November 2007.